Investigation of steady-state tokamak issues by long pulse experiments on Tore Supra

G. Giruzzi, R. Abgrall[3], L. Allegretti, J.M. Ané, P. Angelino, T. Aniel, A. Argouarch,
J.F. Artaud, S. Balme, V. Basiuk, P. Bayetti, A. Bécoulet, M. Bécoulet,
L. Begrambekov[14], M.S. Benkadda[16], F. Benoit, G. Berger-by, B. Bertrand,
P. Beyer[16], J. Blum[9], D. Boilson[15], H. Bottollier-Curtet, C. Bouchand, F. Bouquey,
C. Bourdelle, F. Brémond[4], S. Brémond, C. Brosset, J. Bucalossi, Y. Buravand,
P. Cara, S. Carpentier, A. Casati, O. Chaibi, M. Chantant, P. Chappuis, M. Chatelier,
G. Chevet, D. Ciazynski, G. Ciraolo[17], F. Clairet, J. Clary, L. Colas, Y. Corre,
X. Courtois, N. Crouseilles[6], G. Darmet, M. Davi, R. Daviot, H. De Esch, J. Decker,
P. Decool, E. Delchambre, E. Delmas, L. Delpech, C. Desgranges, P. Devynck,
L. Doceul, N. Dolgetta, D. Douai, H. Dougnac, J.L. Duchateau, R. Dumont,
G. Dunand, A. Durocher, A. Ekedahl, D. Elbeze, L.G. Eriksson, A. Escarguel[16],
F. Escourbiac, F. Faisse, G. Falchetto, M. Farge[10], J.L. Farjon, N. Fedorczak,
C. Fenzi-Bonizec, X. Garbet, J. Garcia, J.L. Gardarein, L. Gargiulo, P. Garibaldi,
E. Gauthier, A. Géraud, T. Gerbaud, M. Geynet, P. Ghendrih, C. Gil, M. Goniche,
V. Grandgirard, C. Grisolia, G. Gros, A. Grosman, R. Guigon, D. Guilhem,
B. Guillerminet, R. Guirlet, J. Gunn, S. Hacquin, J.C. Hatchressian, P. Hennequin[12],
D. Henry, C. Hernandez, P. Hertout, S. Heuraux[11], J. Hillairet, G.T. Hoang,
S.H. Hong, C. Honore[12], J. Hourtoule, M. Houry, T. Hutter, P. Huynh, G. Huysmans,
F. Imbeaux, E. Joffrin, J. Johner, J.Y. Journeaux, F. Jullien, F. Kazarian, M. Kočan,
B. Lacroix, V. Lamaison, J. Lasalle, G. Latu[6], Y. Lausenaz, C. Laviron, C. Le Niliot[7],
M. Lennholm, F. Leroux, F. Linez, M. Lipa, X. Litaudon, T. Loarer, F. Lott, P. Lotte,
J.F. Luciani[2], H. Lütjens[2], A. Macor, S. Madeleine, P. Magaud, P. Maget, R. Magne,
L. Manenc, Y. Marandet[16], G. Marbach, J.L. Maréchal, C. Martin[16], V. Martin[4],
A. Martinez, J.P. Martins, R. Masset, D. Mazon, L. Meunier, O. Meyer, L. Million,
M. Missirlian, R. Mitteau, P. Mollard, V. Moncada, P. Monier-Garbet, D. Moreau,
P. Moreau, M. Nannini, E. Nardon, H. Nehme, C. Nguyen, S. Nicollet, M. Ottaviani,
D. Pacella[1], S. Pamela, T. Parisot, H. Parrat, P. Pastor, A.L. Pecquet, B. Pégourié,
V. Petrzilka[5], Y. Peysson, C. Portafaix, M. Prou, N. Ravenel, R. Reichle, C. Reux,
P. Reynaud, M. Richou, F. Rigollet[7], F. Rimini, H. Roche, S. Rosanvallon, J. Roth[13],
P. Roubin[16], R. Sabot, F. Saint-Laurent, S. Salasca, T. Salmon, F. Samaille,
A. Santagiustina, B. Saoutic, Y. Sarazin, J. Schlosser, K. Schneider[17], M. Schneider,
F. Schwander , J.L. Ségui, J. Signoret, A. Simonin, S. Song, E. Sonnendruker[6],
P. Spuig, L. Svensson, P. Tamain, M. Tena, J.M. Theis, M. Thonnat[4], A. Torre,
J.M. Travère, E. Trier[12], E. Tsitrone, F. Turco, J.C. Vallet, A. Vatry, L. Vermare[12],
F. Villecroze, D. Villegas, D. Voyer[8], K. Vulliez, W. Xiao, D. Yu, L. Zani, X.L. Zou and
W. Zwingmann

CEA, IRFM, F-13108 St Paul-lez-Durance, France
[1] Associazione EURATOM-ENEA sulla Fusione, C.R. Frascati, Roma, Italy
[2] CPT, Ecole Polytechnique, 91128 Palaiseau, France
[3] INRIA–CNRS:UMR5800–CNRS:UMR5466, Université Sciences et Technologies, Bordeaux, France
[4] INRIA Sophia-Antipolis, 2004 Route des Lucioles BP 93, 06902 Sophia Antipolis, France
[5] IPP, Association EURATOM/IPP.CR, Za Solvankou 3, PO Box 17, 18221 Prague, Czech Republic
[6] IRMA, Université Louis Pasteur, Strasbourg, France
[7] IUSTI–CNRS, University of Provence, Marseille, France
[8] Laboratoire Ampère (UMR CNRS 5005), Université de Lyon, Ecole Centrale de Lyon, Ecully, France

[9] LJAD, U.M.R. C.N.R.S. No 6621, Université de Nice, Sophia, Antipolis

[10] LMD–CNRS, Ecole Normale Supérieure, Paris, France

[11] LPMIA, CNRS (UMR 7040), Université Henri Poincaré, France

[12] LPTP, Ecole Polytechnique, 91128 Palaiseau, France

[13] Max-Planck-Institut für Plasmaphysik, EURATOM Association, 85748 Garching, Germany

[14] Moscow Physics and Engineering Institute (MEPhI), 31 Karhirskoe Sh, 115409 Moscow, Russia

[15] School of Physical Sciences, Dublin City University, Glasnevin, EI-Dublin 9, Ireland

[16] Université de Provence/CNRS, Physique des Interactions Ioniques et Moléculaires, UMR 6633, Marseille, France

[17] MSNM-GP, UMR 6181–CNRS/Université Paul Cézanne, Marseille, France

Abstract

The main results of the Tore Supra experimental programme in the years 2007–2008 are reported. They document significant progress achieved in the domain of steady-state tokamak research, as well as in more general issues relevant for ITER and for fusion physics research. Three areas are covered: ITER relevant technology developments and tests in a real machine environment, tokamak operational issues for high power and long pulses, and fusion plasma physics. Results presented in this paper include test and validation of a new, load-resilient concept of ion cycotron resonance heating antenna and of an inspection robot operated under ultra-high vacuum and high temperature conditions; an extensive experimental campaign (5 h of plasma) aiming at deuterium inventory and carbon migration studies; real-time control of sawteeth by electron cyclotron current drive in the presence of fast ion tails; ECRH-assisted plasma start-up studies; dimensionless scalings of transport and turbulence; transport experiments using active perturbation methods; resistive and fast-particle driven MHD studies. The potential role of Tore Supra in the worldwide fusion programme before the start of ITER operation is also discussed.

(Some figures in this article are in colour only in the electronic version)

1. Introduction

Twenty years after the start of its operation (April 1988), Tore Supra remains the only large tokamak fully equipped for steady-state operation, combining superconducting magnetic coils, actively cooled plasma facing components (PFCs) and non-inductive current drive capability. Its primary mission, the investigation of physics and technology issues of steady-state tokamak operation, retains all its scientific interest and relevance to the fusion programme. After the attainment of the symbolic target of discharges with 1 GJ of injected energy (>6 min duration) [1], the next initiative was the systematic increase in the injected power ($\sim$10 MW), on shorter discharges ($\sim$20–30 s, but still significantly longer than the current redistribution time) [2]. This phase allows the exploration of an operational domain of the highest interest for ITER and reactor applications: the combined use of ion cyclotron resonance heating (ICRH) and lower hybrid current drive (LHCD) systems at significant injected energy levels poses specific problems of antenna–plasma edge interactions [3] that can presently be fully tackled on Tore Supra only. The bonus of this class of experiments is related to the simultaneous presence of electron and ion tails in plasmas at $T_i \sim T_e$, which allows the investigation of various ITER relevant fusion physics subjects. Systematic operation of Tore Supra over the past several years at high power levels for long pulses has revealed growing limitations of the power that can be successfully coupled to the plasma. These limitations manifest

themselves as a steadily increasing disruptivity of discharges of the same type, which is believed to be related to the formation of carbon deposits on the PFC. The problem of high power, long pulse operation is therefore tightly related to another ITER relevant subject that constitutes a major part of the Tore Supra scientific programme: erosion and re-deposition processes on PFC and the associated deuterium retention [4]. This was the subject of a specific experimental campaign in 2007.

This work reports the main achievements of the Tore Supra programme in the last two years. Significant results have been obtained in three areas: ITER relevant technology developments and tests in a real machine environment, tokamak operational issues for high power and long pulses, and experiments oriented to fusion plasma physics studies. The potential role of Tore Supra in the worldwide fusion programme before the start of ITER operation will also be discussed.

2. Technology developments

Technology developments for ITER are naturally a significant part of the fusion research proramme. In some cases, it is important to use an existing fusion machine as a test-bed for such developments, in order to check the compatibility with a real machine environment and with plasma operation. In this section, two examples of this type of use of Tore Supra are presented: an ITER-like prototype of ICRH antenna and a newly developed inspection robot.
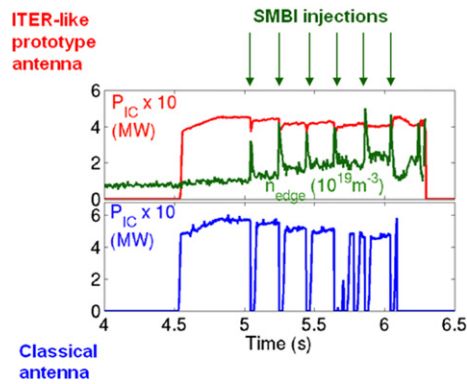
Figure 1. Comparison of the ICRH power injected by the ITER-like prototype antenna (top box) and by a conventional antenna (bottom box), in the presence of density perturbations induced by SMBI (characterized by the edge density behaviour, also shown in the top box).

2.1. ITER-like antenna

ICRH is one of the two main heating systems of ITER. In this respect, the main challenge is the development of ICRH antennas compatible with a reactor environment and resilient to large perturbations of the plasma edge density (especially edge localized modes, ELMs). An ITER-like prototype ICRH antenna for Tore Supra has been developed since 2003 [5] and extensively tested in the 2007 experimental campaign. The design of this prototype is based on the conjugate-T concept proposed for ITER [6] to deal with fast loading perturbations. The prototype launcher consists of two resonant double loop (RDL) antennae arranged toroidally. Compared with the 'conventional' RDL circuit, this RF circuit has the advantage that the antenna sensitivity at large variations of the resistive part of the load is lower.

The experimental test of the antenna on plasma consisted in the study of the load resilience properties of the system, using edge density perturbations produced by pellet or supersonic molecular beam injection (SMBI); qualification of the simulation models used in the design and investigation of the antenna power limits [7]. The most striking demonstration of the load resilience properties of the antenna has been obtained using SMBI to produce fast density perturbations on the injected power, coupling resistance R_c and reflected power, on both the ITER-like and a conventional antenna simultaneously. This is illustrated in figure 1. In the same discharge, on the classical RDL antenna any of the SMBI injections triggers the safety system switching the applied power off, whereas with identical safety conditions for the generator, the ITER-like antenna couples its power to the plasma without interruption [7]. The coupling properties of the antenna have been compared with RF circuit calculations that include 3D modelling for the complex structures. During a single shot the plasma position varies over a large range (60 mm), and the voltage standing wave ratio (VSWR) is plotted against the coupling resistance in figure 2. The shot covers the low and the high parts of the R_c value, respectively. The agreement with the expected computed behaviour of the ITER-like antenna is very satisfactory.

The last part of the campaign was dedicated to technical tests, with the objective to power the antenna up to its limits.
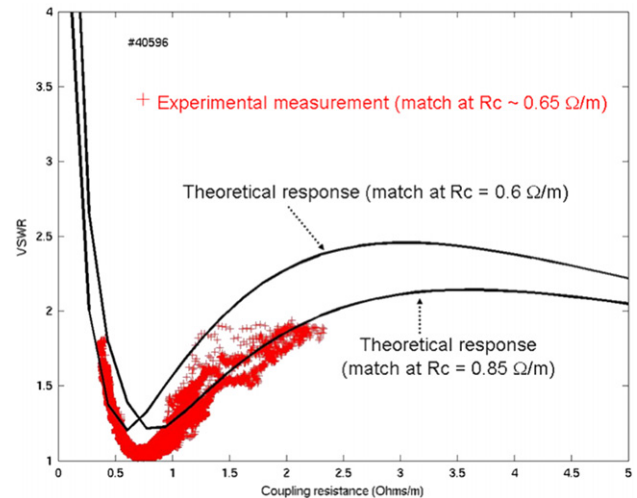

Figure 2. Shot 40596: VSWR as a function of the coupling resistance: experimental data from a single discharges (symbol: +); electrical simulation (bold lines).

The maximum power reached was 2.2 MW, with 36 kV on the straps. In order to reach such a power level, several hours of RF conditioning were necessary. This process was far longer on the ITER-like prototype structure, that features small conductors inter-spacing along the vacuum transmission line under vacuum, than on a RDL structure. Repetitive conditioning shots with power steps of 100 kW were required to reach the electrical limits. The performance in terms of coupled power and pulse duration could be optimized, in terms of Faraday screen and antenna box, therefore the resulting coupling resistance is expected to be limited both by the vacuum transmission line design and by the internal component design (current strap geometry in particular). These results represent a significant milestone towards future integration of ICRH launchers on ITER. The next step is the validation of the same concept on a larger scale and with an ELMy plasma on JET, which is presently underway.

2.2. Articulated inspection arm (AIA)

A very important issue for long pulse operation and for ITER is the monitoring of the inner components degradation, with thorough visual inspection (without breaking the machine vacuum and conditioning) as a first step. For this purpose, an AIA has been developed, to demonstrate the feasibility of an in-vessel remote handling inspection carrier, with limited payload (10 kg) [8]. The AIA robot is an 8 m long, multi-link carrier composed of five identical modules of 160 mm diameter with two electrical joints. The robot is translated along its support with an additional linear joint called the deployment system. The size of the AIA robot demonstrator is similar to what could be used in ITER. The operating conditions are ITER relevant, with ultra-high vacuum and 120 °C temperature compatibility, but interventions under magnetic field are not possible with the technologies implemented on this robot. After several experiments on a dedicated test facility, the robot has been installed on Tore Supra and equipped with a high definition CCD camera for PFCs visual inspection (figure 3). The viewing system is cooled with nitrogen gas in order to

Figure 3. The AIA inside Tore Supra, during an inspection in ultra-vacuum and at 120 °C.

Figure 4. Pulse duration (*a*), number of UFOs per discharge (*b*) and disruption frequency (*c*) versus discharge number. The vertical line indicates the change in the heating scenario (from a square waveform to a continuous ramp of the LH power).

keep the embedded electronic temperature below 60 °C. The tests of deployment in Tore Supra, under ultra-high vacuum (1.4×10^{-5} Pa) and at a temperature of 120 °C have been performed in September 2008. The main motivations of this experiment were the verification of the reliability of the arm movements and an extensive test of the outgassing of the whole structure, which could cause pollution of the plasma in subsequent machine operation. The arm has been fully unfold in the equatorial plane, with additional movements upwards (inspection of an infrared (IR) endoscope shutter) and downwards (close inspection of the toroidal limiter). The duration of the deployment and inspection phase was of the order of 6 h: during this time, the evolution of the various gases in the vacuum chamber has been continuously monitored by spectrometry analysis, without showing any significant variation. These tests [9] have been successful and have demonstrated that previous baking of the arm at 200 °C efficiently limits outgassing during the deployment inside the machine. After the deployment, normal plasma operation has been possible without any particular wall conditioning.

3. Operational issues

3.1. Deuterium inventory

In-vessel tritium retention is a crucial issue for ITER since a simple extrapolation of present measurements shows that the limit of 700 g set by nuclear licensing could be reached within a few hundreds nominal discharges for the reference wall materials combination (carbon fibre composite at the divertor target strike point/tungsten dome and upper divertor targets/beryllium first wall) [10]. Although the general trends regarding hydrogenic retention are well established and observed in many devices, the relative contributions of the underlying physical processes have not been clearly identified and retention rates deduced from integrated particle balance ($\sim$10–20% of the injected gas, >30% in Tore Supra) are significantly larger than those estimated from post-mortem analysis of the PFCs ($\sim$3–4%) [11]. Comparing these two estimates is difficult, since the former is generally based on particle balance calculations for a limited number of discharges, whereas the latter integrates the whole history of the PFCs. To clarify where the missing deuterium is trapped, the best approach is to load the wall with deuterium in a controlled discharge scenario until its inventory is known with
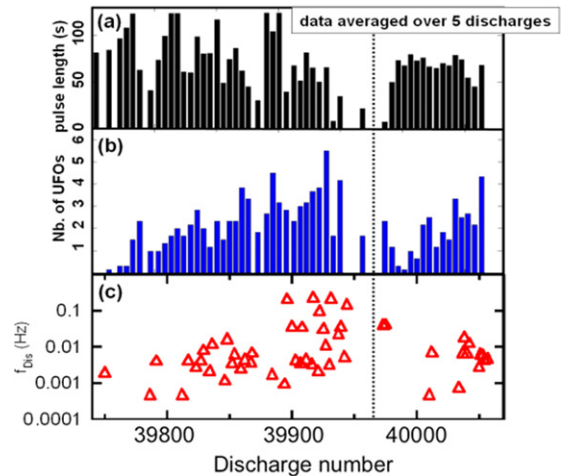
a sufficient accuracy from integrated particle balance, and then to dismantle some of the PFCs for analysis. Such a study was undertaken on Tore Supra, in three phases: a dedicated campaign to load the PFCs with deuterium, the dismantling of a toroidal limiter sector to extract selected samples, and then an extensive analysis programme on the samples, in collaboration with European partners in the frame of the European Plasma Wall Interaction Task Force [12, 13].

At the start of the experiment, the vessel was carbonized, then boronized in order to mark the beginning of the experiment by a ^{13}C-layer, easily identifiable in subsequent analysis, and for initial wall conditioning. A robust scenario was designed to allow plasma duration long enough ($\sim$2 min) for permanent retention to be much larger than the transient one, namely average density $\langle n_e \rangle = 1.5 \times 10^{19}$ m^{-3}, LH power $P_{LH} = 2$ MW, plasma current $I_p = 0.6$ MA and magnetic field $B_T = 3.8$ T. Ten days of operation were devoted to the D-loading of the wall ($\sim$5 h of plasma, equivalent to approximately 1 yr of normal operation). Neither of the other experimental programmes, nor wall conditioning were carried out during this time. The main operational issue was linked to the appearance of UFOs (i.e. large particles with a high impurity content, detached from the wall, PFCs or antennas, and penetrating into the plasma), whose frequency increased dramatically during the campaign, triggering a phase of plasma detachment followed by a disruption in a number of cases [14, 15]. This is shown in figure 4, where the number of UFOs per discharge is plotted versus the discharge number, showing an almost linear increase and a correlated decrease of the plasma duration. In order to overcome this limitation, it became necessary to modify the LH power waveform, from its initially constant value to a continuous ramp, from 1.2 to 1.6–1.8 MW, and also to decrease the plasma duration down to $\sim$80 s (this change corresponds to the vertical line in figure 4). The continuous increase of the UFO frequency is believed to be related to the build-up of thick deposits in the shadowed regions of the toroidal surface—in the immediate vicinity of the confined plasma.
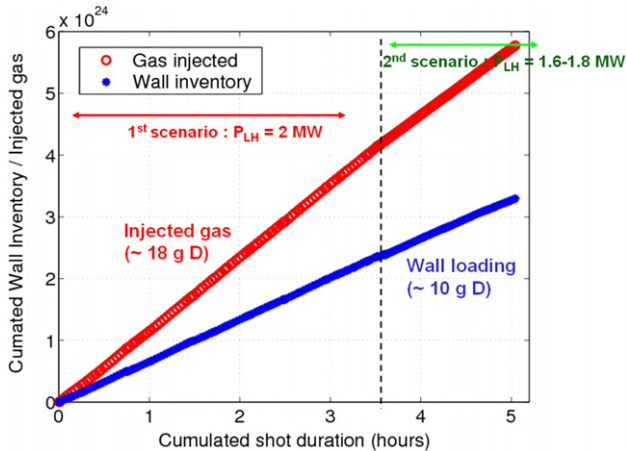
Figure 5. Injected gas and wall D inventory versus cumulated discharge duration for the dedicated campaign.
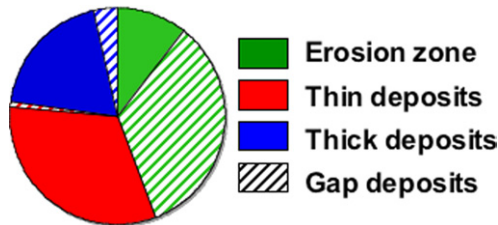

Figure 6. Breakdown of the D-content in the different zones (thick deposits, thin deposits, erosion and gaps), as determined by TDS and NRA.

The main results of particle balance are presented in figure 5, where the injected gas and the wall D inventory are plotted versus the cumulated discharge duration. A constant retention rate was measured ($\sim 2 \times 10^{20}$ D s^{-1} in the stationary phase), with no sign of wall saturation, leading to a total increment of the wall inventory of $\sim 3 \times 10^{24}$ D (~ 4 times the pre-campaign estimate). After dismantling a sector of the toroidal limiter (20° toroidal), 40 CFC-tiles (out of a total number of 672 for the whole sector)—distributed over erosion, thin-deposit and thick-deposit zones—were extracted for analysis. Thermodesorption (TDS) and nuclear reaction analysis (NRA) measurements of the D-content were performed on a first selection of tiles. These measurements showed surface D-concentration of $\sim 5\%$ and $\sim 20\%$ in the eroded and deposition zones respectively, on a typical thickness of 10 to 40 μm [12]. As shown in figure 6, once extrapolated over the whole limiter, this corresponds to $\sim 50\%$ of the total inventory, mainly determined by the deposition zones and gaps between tiles [13]. It is found that the retention process is dominated by codeposition; approximately 10% of deuterium penetrates in the erosion zones, owing to the high porosity of the CFC material. These results have of course a strong impact on the subsequent choices of detritiation techniques, at least for carbon-based PFCs, since such techniques will depend on the location of the deposits.

3.2. High power issues

The recent experimental campaigns have been particularly intense in terms of injected power, energy and accumulated

plasma time (10 h plasma time in both 2006 and 2007, with 65 GJ injected RF energy in 2006 and 40 GJ in 2007). Significant experience has been gained in the understanding of localized heat loads due to RF sheath effects and interaction of fast particles [3, 14]. In addition to the previously discussed scenario with LH only, developed for D-retention studies, high power scenarios have also been explored, combining LHCD and ICRH, at higher plasma current and density ($I_P = 0.9$ MA and $n_e/n_{Gr} \sim 0.8$). During the 2006 campaign, this scenario yielded ~ 10 MW coupled for 26 s in repetitive discharges [14]. However, as in the D-retention campaign, an increasing operational difficulty emerged, limiting the high power and long pulse performance. The analyses undertaken suggest that the limitation is linked to the growth and flaking of re-deposited carbon layers on the main PFC. This type of operational limit encountered on Tore Supra could represent a serious concern for next step devices that operate repetitive discharges over long durations, leading to re-deposited layers of significant thickness.

In order to understand the dynamics of these disruptive limits, the pre-disruption behaviour of more than 140 discharges from the 2006 and 2007 campaigns have been analysed [15], using IR imaging together with visible and ultraviolet (UV) spectroscopy of impurities (carbon, iron and oxygen). The IR images reveal in several cases the appearance of a small ($\sim$cm^2) hot spot, clearly localized in a zone of thick carbon re-deposition ($>100\,\mu$m) on the main PFC, the toroidal limiter. At the hot spot, the surface temperature increases by a few hundred degree celsius, lasting several time frames (>50 ms) until the plasma disruption. Ejection of flakes from the re-deposition zones is observed by the IR as well as CCD cameras and is associated with the formation of a MARFE. The most likely mechanism is the continuous growth of the carbon deposits, resulting from over 44 h accumulated plasma time since the installation of the toroidal limiter in 2000. As the deposits are heated up by plasma radiation, they tend to crack and partially detach from the surface, the thermal resistance between the deposits and the actively cooled surface increases, thus heating the deposits even further. Eventually, flaking occurs as a result of inner thermal stresses, and UFOs are formed. This mechanism, likely responsible for the new operational limit encountered, does not seem specific to C-based PFCs: it could be found for other types of deposited layers (e.g. Be), with bad thermal contact with the actively cooled PFC.

To validate this hypothesis, the carbon deposits on the PFCs were completely removed during the winter shutdown 2007–2008. This was a complex intervention, lasting 10 days. It was performed by hand by four teams of two people, equipped with gas masks for protection against carbon dust inhalation, and using tungsten carbide scrapers and vacuum cleaners (~ 0.8 kg of carbon has been recovered and is available for analysis). This thorough cleaning procedure had a dramatic impact on the operation of the machine. After ohmic restart, LH, then ICRH power increase phases have been performed (this took typically four operation days, including antenna conditioning on plasma discharges). After a boronization, high power operation with combined LH and ICRH power was commenced—usually a very lengthy procedure in the presence of carbon deposits. This time, nine discharges were sufficient
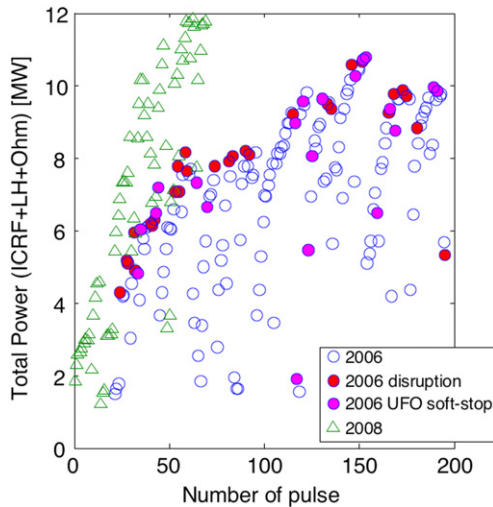
Figure 7. Total additional power versus the number of pulses realized for a power increase phase in 2006 (circles) and in 2008 (triangles).
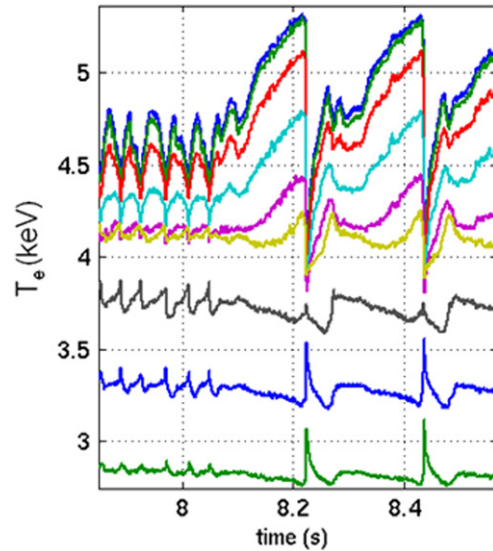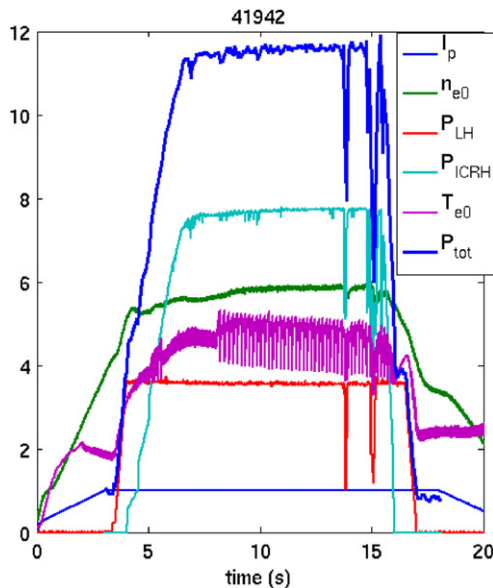

Figure 8. Time history of a 12 MW discharge, obtained after PFC cleaning. Powers are in MW, current in MA, density in 10^{19} m^{-3}, temperature in keV.

Figure 9. Time behaviour of the central ECE channels for the discharge of figure 8.

demonstrates the importance of the PFC cleaning procedure (or of preventing the formation of deposits) for successful operation of long pulse tokamaks.

The high power discharge shown in figure 8, as well as several other discharges of the same type, exhibits a peculiar behaviour: spontaneous transitions are observed in the sawtooth amplitude and period, at constant heating power and often without noticeable changes in the macroscopic plasma parameters (density, q profile). An expanded view of several electron cyclotron emission (ECE) channels versus time, for the transition at 8 s of the discharge of figure 8, is shown in figure 9. It is remarkable that practically no intermediate level of sawtooth period and amplitude has been observed in the discharges featuring such a transition: the systems has a sort of bi-stable behaviour. Since these sawteeth are stabilized by the fast ion tail produced by ICRH minority heating, the transitions observed are likely related to the distribution of the fast ions and to the MHD phenomena driven by them. These phenomena, which have to be further investigated, may have an impact on the sawteeth control techniques, which can be employed in high power discharges, in particular in the ITER reference scenario.

3.3. Real-time sawtooth control by electron cyclotron current drive (ECCD)

Fast ions—such as fusion produced alpha particles in future reactors or ICRH accelerated ions in present tokamaks—stabilize the 'sawtooth' instability, resulting in long sawteeth with large crashes, which are prone to trigger neoclassical tearing modes (NTM). Thus NTMs may be avoided if short sawteeth can be maintained, even in the presence of significant fast ion pressure, and ECCD is foreseen to accomplish this function on ITER, by driving localized currents close to the $q = 1$ surface and therefore changing the magnetic shear locally. On Tore Supra, experiments have been performed to demonstrate ECCD destabilization of sawteeth in the presence of fast ion tails produced by ICRH, for the first time. These
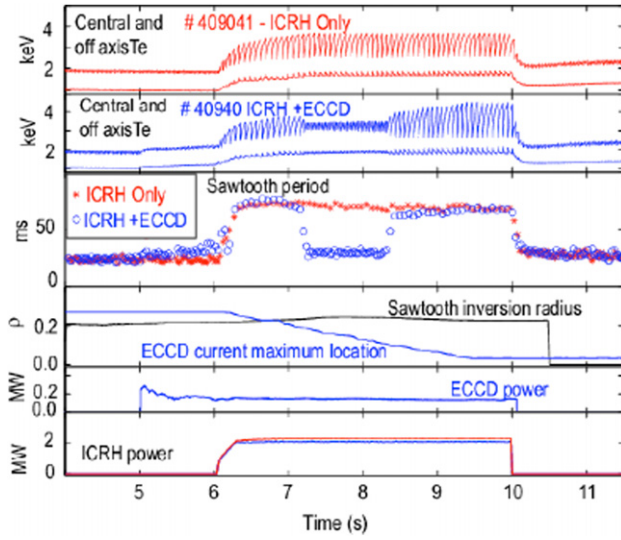
to attain a total power of 11 MW, without any disruption. In a subsequent day, this power level could be attained in 3 shots. No signs of the previously observed phenomenology (hot spot, flaking, MARFE, disruption) have been observed in all the restart and power increase phases. A comparison of this power increase phase with a typical one in the presence of carbon deposits (2006) is shown in figure 7. It is apparent that the power increase is much faster, due to the absence of disruptions and of UFOs. Note that the impurity content is globally very similar in the two campaigns, for similar discharges. As a result, no particular effort was required to obtain a discharge with nearly 12 MW of total heating power (very close to the maximum power presently available on Tore Supra), for a duration of 10 s (figure 8). This result opens up promising prospects for the future power upgrade of Tore Supra. It also

Figure 10. Comparison of two consecutive shots—one with 2.3 MW of ICRH and no ECCD and one with ECCD added. From top to bottom: temperatures, sawtooth periods, ECCD and inversion radius locations, powers.

Figure 11. Sawtooth period versus distance between the ECCD location and the inversion radius, for co- and counter-ECCD. (*a*) and (*b*) show the result with central ICRH and in ohmic plasma, respectively.

Figure 12. Feedback control of the sawtooth period using the poloidal injection angle of the ECCD as an actuator. Note that changes of the sawtooth period after the end of the feedback phase are due to variations of the ICRH power.

experiments include demonstration of co- and counter-ECCD effects on the sawtooth period [16], as well as feedback control of the sawtooth period by moving the steerable mirrors of the ECCD antenna in real time [17], as foreseen in ITER. An example of the effect of ECCD on the sawtooth period is shown in figure 10. During the ICRH phase ($P_{ICRH} = 2$ MW) of a 1 MA discharge, co-ECCD is applied ($P_{ECCD} \approx 0.2$ MW) at a toroidal injection angle of $28°$, while the poloidal injection angle is continuously swept from $-3°$ to $-8°$ in order to move the driven current location through the $q = 1$ surface. This results in a strong and abrupt decrease of the sawtooth period in a well defined time window. For comparison, it is interesting to consider the effect of counter-ECCD. Figure 11 shows the sawtooth period as a function of the distance between the inversion radius and the peak of the ECCD deposition, for a number of discharges, similar to the one shown in figure 10, with both co- and counter-current ECCD. Shortening of the sawtooth period is achieved with the ECCD current driven inside and outside the $q = 1$ surface, for co-and counter-ECCD, respectively. The lower panel of figure 11 also shows that the ECCD has very little effect on the sawtooth period in ohmic plasmas. The abrupt switch of the sawtooth period is analogous to the bi-stable behaviour observed in the spontaneous transitions, which leads us to conjecture that, in the presence of fast ions, other mechanisms in addition to the evolution of the shear at $q = 1$ must be invoked to explain the experimental results.

In the present set of experiments a simple closed loop controller for real time control of the sawtooth period was implemented [17]. Such a control will be required in future machines for sawtooth destabilization to be a viable option for NTM avoidance. These experiments were successful in proving that the sawtooth period can be switched reliably between short and long sawteeth though they also highlighted the difficulty associated with the abrupt change in sawtooth period. As shown in figure 12, the controller has not been able to obtain an intermediate state between the long (~70 ms)
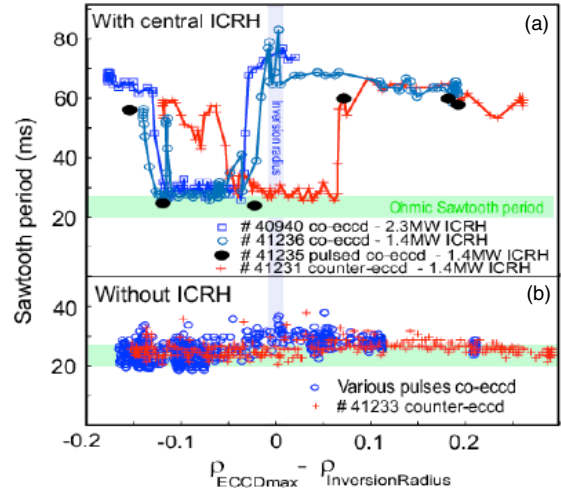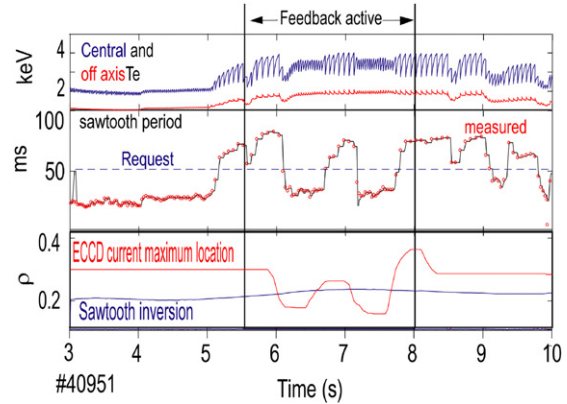
and the short (~30 ms) sawtooth period. If this bi-stable behaviour is universal—as it seems to be at present—the control algorithms implemented on future tokamak devices must take this into account and better physics understanding of this phenomenon would be very helpful for the success of such control schemes.

3.4. ECRH-assisted start-up

ECRH pre-ionization and assisted start-up will be necessary in ITER [18]. The use of superconducting poloidal field coils will limit the available toroidal electric field ($E_T \leqslant 0.3$ V m^{-1}), while the presence of toroidally continuous vacuum-vessel structures will increase the magnetic 'stray' field (axisymmetric poloidal fields normal to the toroidal field B_T) at breakdown. With this motivation, experiments aiming at ECRH-assisted start-up for electric field values close to the ITER limit have been performed on Tore Supra [19]. ECRH at the 1st cyclotron harmonic, O-mode polarization (as presently foreseen in ITER) has been applied for typically
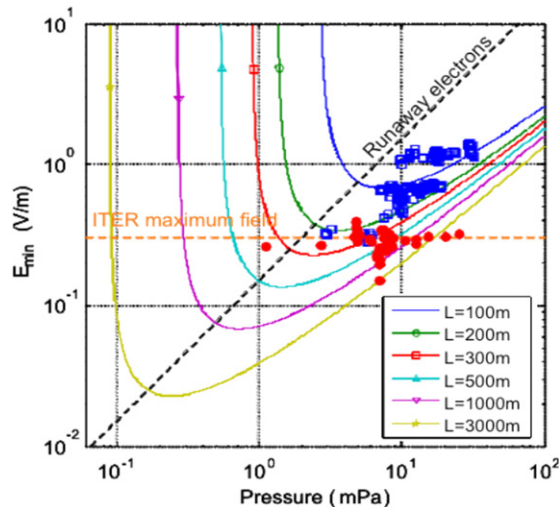
Figure 13. Applied electric field versus pre-fill pressure for a number of successful start-up attempts, both with and without ECRH assistance. Open squares correspond to ohmic startup, full circles to ECRH-assisted startup. *L* is the toroidal connection length. Townsend curves are also shown.

50 ms, using one or two 118 GHz gyrotrons (P_{EC} = 300–500 kW), at oblique injection (toroidal angle ∼30°). The usual start-up voltage on Tore Supra is 25 V (E_T = 1.7 V m^{-1}) with deuterium pre-fill pressure around 20 mPa. The minimum stray field value (B_∞) in most of the vacuum vessel is lower than 5 mT, which gives toroidal connection lengths ($L = aB_T/B_\infty$) longer than 770 m. In these conditions, pre-ionization was successfully achieved at the EC resonance location and <30 kA of current was established in 10 ms. Successful plasma initiation has been obtained down to <0.15 V m^{-1} at 7 mPa. ECRH-assisted start-up has also been regularly employed at plasma restart after two machine shut-downs of several months, with major loss of conditioning due to various operations inside the vacuum vessel, including PFC cleaning. ECRH has proven to be a very reliable and useful tool for plasma start-up in such difficult conditions [19]. A global plot of the successful start-up attempts at low loop voltage is presented in figure 13. It appears that with ECRH startup at a globally lower electric field is achieved.

4. Fusion physics-oriented experiments

4.1. Dimensionless scalings

A substantial amount of experimental time has been devoted to physics-oriented investigations. The basic dependences of heat transport coefficients on dimensionless quantities (β, ρ^* and ν^*) have been investigated in L-mode discharges in which two of the three quantities were kept fixed, not only in their average values but also, as far as possible, in their radial profiles. The key feature of these studies is that turbulence measurements have been systematically performed in the same discharges, using two types of reflectometers (fast sweeping and Doppler) [20]. In this way, global scaling laws have been compared with those of the local transport coefficients and of the turbulence profiles. Results on the β scaling have been presented elsewhere [20, 21]. The main interest for studying

L-mode scaling laws is to compare them to H-mode scalings determined e.g. in JT-60U [22], ASDEX Upgrade [23] and JET [24]. This allows one to identify the role of edge phenomena, such as ELMs and pedestal physics.

More recently, experiments have been carefully performed by varying the dimensionless collisionality parameter, ν^*, by a factor ∼4.5 [25]. This has been accomplished by magnetic field variations in the range 2.4–3.87 T, with appropriate adjustments of current and ICRH power, in order to keep q, β and ρ^* fixed. Density fluctuations ($\delta n/n$), measured by both reflectometers, are found to increase significantly when increasing ν^* in the outer part of the plasma, as illustrated in figure 14 for four discharges characterized by values of ν^* at mid-radius in the range 0.13–0.61. At the same time, the global confinement time degrades ($B_0\tau_E \propto \nu^{*-0.4\pm0.2}$). In contrast, there is no significant modification of $\delta n/n$ in the central region ($r/a < 0.7$). A similar trend is found by local transport analyses, shown in figure 15, where the heat diffusivities are represented using the same symbols as in figure 14. As compared with previous L-mode experiments performed in TFTR [26] and DIII-D [27] in which no dependence has been found, these new results exhibit a mild ν^* dependence of the global confinement time. This behaviour suggests that the ν^* dependence in L-mode may differ from a power law.

4.2. Perturbative transport studies

Transport studies using active perturbation methods have been carried out, for heat, particles and impurities. In particular, ECRH power modulations at low frequency (1 Hz) have been used to investigate the controversial subject of heat pinch, which has been observed in some experiments [28].

Perturbation techniques have also been used to study the dependence of impurity transport on the atomic number Z and on electron heating. Different metallic impurities (in the range Z = 13–32) have been injected in ohmic, sawtooth-free plasmas using laser blow-off techniques, and the associated response has been observed on the soft x-ray tomography and UV spectroscopy signals [29]. In ohmic discharges, the Z range has been extended by studying nitrogen transport using SMBI of small traces of the impurity [30]. This allows repeated injections in the same pulse, reducing the statistical uncertainties of the results, without increasing the injected amount of atoms above the trace level. Combination of these transient measurements with standard stationary transport analysis (which is used as a constraint on the pinch velocity to diffusion coefficient ratio V/D) has allowed further reduction on the uncertainty of the determination of both D and V, as shown in figure 16. The experimental diffusion has been found to be anomalous everywhere and independent of Z; for nitrogen, the convection is inwards. Modelling using the quasilinear gyrokinetic code QuaLiKiz [31] predicts that (i) transport is governed by ITG turbulence even close to the plasma centre, (ii) the turbulent V (matching the experimental profile shape) is inwards, because the outward thermodiffusion term is weaker than the inward curvature term, (iii) the Z dependence of V is weak in the Z range investigated.

4.3. Sol physics

Various phenomena occurring in the scrape-off-layer of Tore Supra have also been investigated: ion temperature
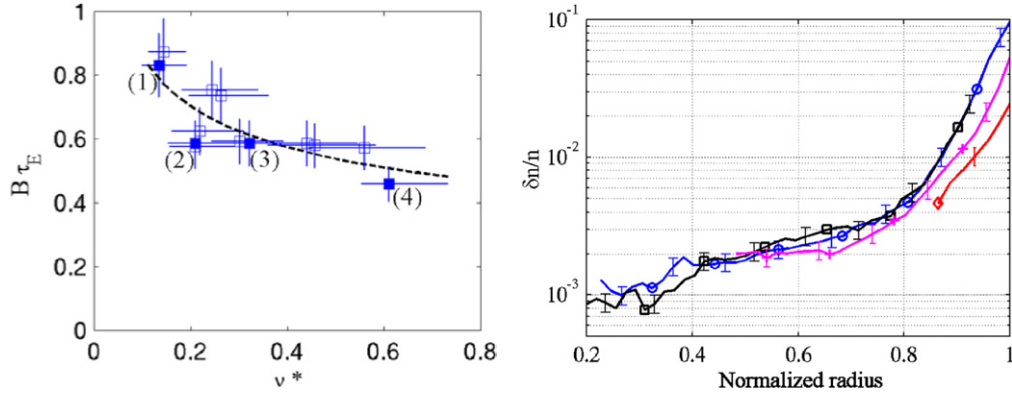
Figure 14. Left: energy confinement time behaviour versus collisionality. Right: radial profiles of density fluctuations $\delta n/n$ for discharges with different ν^* (diamonds: $\nu^* \sim 0.13$; plus: $\nu^* \sim 0.20$; circles: $\nu^* \sim 0.32$, squares: $\nu^* \sim 0.61$, labelled as 1, 2, 3, 4 in the left panel).
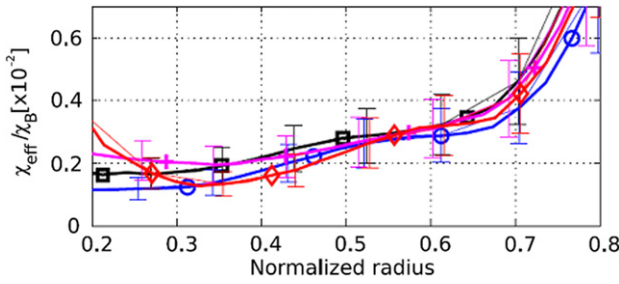

Figure 15. Effective heat diffusivity (normalized to the Bohm diffusivity) determined from experimental data for the four discharges of figure 14 (same symbols).

scaling [32], sheath potentials generated by RF antennae and superthermal electron acceleration [33]. To this end, highly reliable scenarios have been developed to allow, for example, detailed radial–poloidal mapping of the antenna–SOL interaction zones in a single shot, using a retarding field analyzer (RFA) or Mach/tunnel probe. Up to 14 reciprocations 1–2 cm inside the last closed flux surface (LCFS) at a rate of 1 Hz have been made in a single full power discharge. Real-time feedback on edge safety factor is used to vary the magnetic connection between the probe and any of the antennae. The probe position itself is controlled by feedback on real-time magnetic reconstruction to guarantee safe, reliable, and reproducible operation. This technique was used during LHCD experiments to provide direct measurements of the particle and power fluxes of suprathermal electrons emanating from the region in front of the LH grill. When one of the active waveguide rows of the LH launcher is magnetically connected to the RFA, a strong particle flux due to suprathermal electrons is observed. Surprisingly, the radial width of the suprathermal electron beam is rather large, at least about 5–6 cm (figure 17). Theory predicts that the high $n_{\parallel}$ (parallel refractive index) waves (whose spectrum depends mainly on waveguide geometry) should be totally absorbed within at most 5 mm, and that the electron current should be stationary in time [34]. In reality, it exhibits a highly intermittent temporal evolution, with a characteristic burst rate in the 10 kHz range. The time scale of the intermittency is reminiscent of SOL turbulence. These measurements suggest that theory needs to identify a mechanism for power
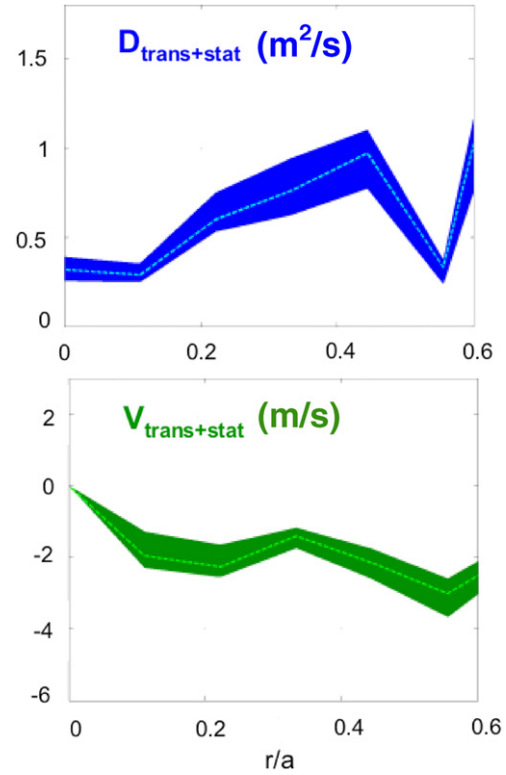

Figure 16. Nitrogen D (top) and V (bottom) profiles, obtained by the transient + stationary method.

transfer from the main spectral peak to high refractive index at arbitrary distances from the grill, perhaps based on density perturbations. If such a mechanism is indeed at work, it could resolve the persistent inability of present theory to explain the strong increase of localized SOL heating with density. Furthermore, the existence of a power channel from low to high harmonics (such as parametric decay) could provide an alternative to toroidal upshift in the longstanding spectral gap problem.

4.4. MHD: double tearings and non-linear simulations

MHD instabilities specifically affecting steady-state discharges have been thoroughly investigated on Tore Supra for
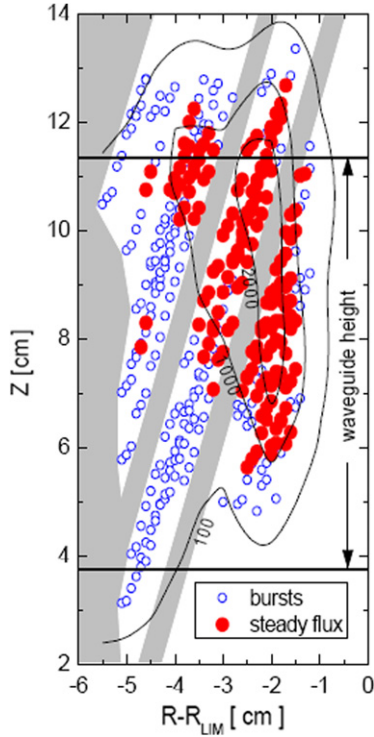
Figure 17. Composite mapping of the flux of electrons with parallel energy greater than 200 eV for LH power = 1.5 MW. Radial distance is measured with respect to the leading edge of the antenna electron-side limiter. All data are shifted vertically to lie in front of the second waveguide row. The horizontal black lines indicate the top and bottom walls of the waveguides. Areas where no data were measured are coloured grey. Full and open circles represent, respectively, points where the time-averaged electron current was lower than $-50\,\mu$A or where 10% of the electron bursts were lower than $-20\,\mu$A. Approximate contours of time-averaged electron current density (A m^{-2}) are shown.

several years. The most familiar MHD activity that is prompt to develop in hollow current density discharges is the double-tearing mode, which is associated with a large variety of experimental observations. Indeed, this mode is seen to produce either off-axis temperature crashes, or to saturate at large amplitude with strong impact on the global confinement, in a behaviour called MHD regime in Tore Supra [35]. Detailed comparisons between experimental observations and predictions by the 3D non-linear MHD code XTOR [36] have been carried out to gain insight into the physics of these different regimes [37, 38]. Non-linear simulations recover both the off-axis and the global crashes, as an effect of the different width of the reconnected region, in a way that is consistent with a full reconnection model (figure 18). Regimes with periodic relaxations or saturation are found to be related to the radial position of the $q = 2$ surface: when moving outwards, the configuration goes from a double-tearing mode which periodically removes the $q = 2$ surface by producing full reconnection, to a single tearing that saturates with a large island and a radial transport that prevents the core pressure to recover (figure 19). The agreement between experiment and simulation is reasonably good whenever the $n = 1$ mode is unstable. However, it appears that successful non-inductive discharges without detectable $n = 1$ mode cannot be reproduced if realistic heat transport coefficients are used in the
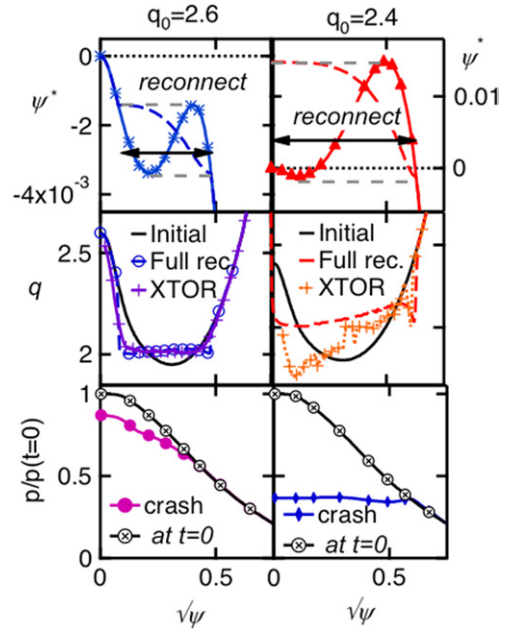

Figure 18. Off-axis and global crash associated to the full reconnection of the double-tearing mode. Reconstructed experimental profiles and XTOR simulations.
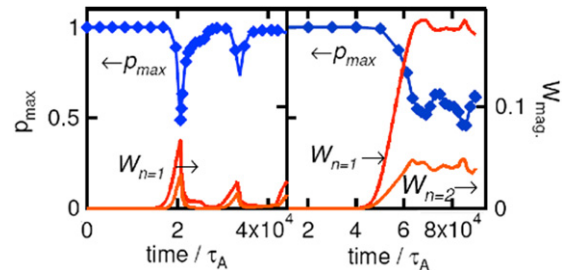

Figure 19. Non-linear simulation of $q = 2$ sawtooth regime and (2, 1) mode saturation with XTOR

simulation. A more comprehensive MHD model implementing diamagnetic effects may provide a non-linear saturation mechanism at small island width.

The transition to the MHD regime has also been investigated by active perturbations of the current density profile by means of ECCD [39]. LHCD discharges at vanishing loop voltage have been perturbed by EC power ($P_{EC} \sim 700$ kW at 118 GHz, O-mode, 1st harmonic) supplied by two gyrotrons, delivering either co- or counter-EC current at different radial locations ($0.05 < \rho_{ECCD} < 0.52$). The current profile evolution has been systematically reconstructed by means of the integrated modelling code CRONOS [40]. Modes frequency and structure, as well as experimental magnetic island width, could be evaluated using the fast-acquisition ECE data. This analysis has shown that the dynamical behaviour of the q profile plays a critical role in the transition: discharges with very similar q profiles evolve towards the MHD regime if the q profile is shrinking, i.e. if the intersections with a given rational surface get closer. This property could be the basis to develop a scheme to prevent the transition to the MHD regime, possibly within a feedback control loop.
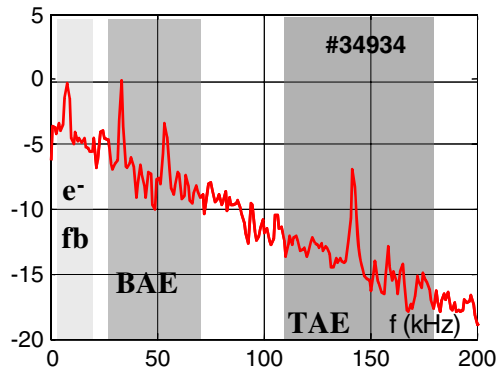
Figure 20. Example of a high frequency modes spectrum observed with reflectometry ($r/a \sim 0.3$) in a LH + ICRH discharge.

4.5. MHD: fast ion and electron modes

Owing to the presence of fast electron and fast ion tails in high power discharges, MHD instabilities associated with fast particles are systematically observed by X-mode reflectometry, fast ECE and correlation ECE. The combination of LHCD and ICRH allows fine tuning of q profile and fast ion populations, which has allowed studies of the radial profile of various modes [41]. It is found that the modes excited cover a wide frequency range from few kHz up to 200 kHz, as shown in figure 20. Electron fishbones have been observed in LHCD plasmas below 20 kHz. Modes around 50 kHz have been identified as beta Alfvén eigenmodes (BAEs) [19]. Toroidal-Alfvén-eigenmodes (TAEs) are also observed in plasmas with ICRH [42, 43]. The frequency range 30–50 kHz corresponds to the acoustic frequency. In this domain, both geodesic acoustic modes (GAMs) and BAEs are expected. However, density perturbations associated with GAMs are predicted to vanish in the equatorial plane, whereas such perturbations are clearly measured there by reflectometry. It is found that the experimental mode frequency follows the BAE dispersion relation. Also the excitation threshold is found to be in reasonable agreement with the experimental observations.

In LHCD discharges, coherent modes at frequencies between 3 and 20 kHz are observed with ECE and reflectometry diagnostics [44]. The mode radial structure and parity are determined using fast ECE acquisitions. Modes are usually localized around $r/a \sim 0.2$ and exhibit an odd parity with respect to the magnetic axis. Information on the q profile is obtained from reconstructions by the CRONOS code [40], using the hard x-ray measurements to constrain the LH absorption profile. Information on the toroidal mode structure is provided by correlating reflectometry and ECE diagnostics located 60° apart in the equatorial plane. The evolution of the MHD stability when varying the LH power has been studied. Two classes of modes have been identified. The first class is characterized by a frequency range 8–10 kHz, consistent with an estimate of the precession frequency for barely trapped fast electrons. Hence these modes have been identified as precessional electron fishbones [45]. The second category of modes, whose frequency is around 2–4 kHz, are likely diamagnetic electron fishbones, since their frequency follows the thermal electron temperature and not the suprathermal energy. In the presence of precessional fishbones the electron temperature exhibits an oscillating behaviour ($\Delta T_e/T_e \sim 1\%$)
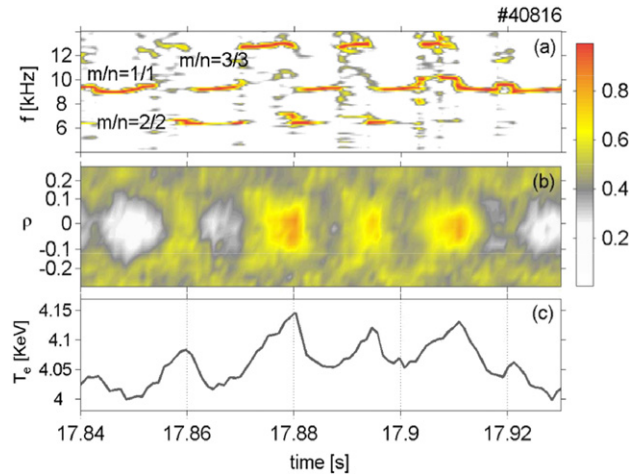

Figure 21. (*a*) Spectrogram of detected modes. (*b*) 2D-surface representing the evolution of the electron temperature $T_e - \langle T_e \rangle$. (*c*) Central electron temperature time trace.

which seems strongly related to the discontinuous evolution of the mode frequency (figure 21). This observation could be at the root of new interpretations of non-linear temperature oscillations first detected in Tore Supra during long pulses [46]. For large enough LH power, diamagnetic electron fishbones take over and the electron temperature oscillation disappears. In this regime, when increasing LH power, a frequency rise is observed, in agreement with the theory.

5. Conclusions and prospects

The peculiar complexity of the physics of non-inductive plasmas opens up several domains of additional studies and interesting physics problems, even after twenty years of efforts. The growing importance of this subject for ITER (and even more for DEMO) motivates Tore Supra to continue investigation in this domain with a high priority. The scientific programme of Tore Supra is now close to the beginning of a new phase. Significant progress will be made possible after the LH power upgrade foreseen for 2009–2010 (CIMES project [47]). Now that the key role of PFC cleaning on plasma disruptivity and high power operation has been understood and demonstrated, this power upgrade can be anticipated with enhanced optimism. With a cw LH power in excess of 6 MW, it will be possible to run the $V_{loop} = 0$ discharges at significantly higher plasma current and/or density. Increase in current implies a proportionally higher global energy confinement, whereas increase in density will allow simultaneous coupling of IC waves at high power level. In this parameter range, the LH waves are expected to be absorbed more off-axis and the global confinement to increase, because of the increased extension of the reversed shear region. The establishment of a LHEP regime [48] at significantly higher β should increase the bootstrap contribution and probably favour improved confinement on a broader plasma region. At the same time, the nature of MHD phenomena will change, owing to the increasing role of pressure, and the overall picture and detailed shape of the MHD stability domains is likely to be modified. The regimes of improved confinement

(LHEP [48]), poor stability (MHD regime [35]) and nonlinear oscillating behaviour (O-regime [46]) being very close and even inextricably connected in parameter space, detailed experimental studies, first-principle physics understanding and development of active control techniques will be subjects of intense activity for Tore Supra with the upgraded heating systems configuration.

In the prospect of the ITER steady-state operation phase and of DEMO, it will of course be necessary to address at least the most urgent of these physics issues in machines equipped for steady-state operation, with divertor configuration and a high degree of flexibility. Four tokamaks of this type (EAST, KSTAR, SST-1 and JT-60SA) have been or are being built in Asia, however, it will take several years before they can reach full performance steady-state operation. Tore Supra is a strategic asset for the international fusion programme to bridge this gap. In order to fully exploit the machine potential for steady-state scenario exploration, a flexible current profile control system has been identified as the most useful further enhancement beyond the CIMES project. An ECCD system of 4–5 MW would be a relatively modest but decisive upgrade which would allow Tore Supra to explore the physics of steady-state scenarios in the next years, before the start of ITER operation. Challenging issues, such as the current alignment problem [49] and the real-time control of fully non-inductive plasmas in the presence of strong non-linearities [50] could be addressed by Tore Supra in such an upgraded configuration.

Acknowledgments

References

[1] Van Houtte D. *et al* 2004 *Nucl. Fusion* **44** L11
[2] Giruzzi G. *et al* 2005 *Plasma Phys. Control. Fusion* **47** B93
[3] Colas L. *et al* 2007 *Plasma Phys. Control. Fusion* **49** B35
[4] Tsitrone E. *et al* 2007 *J. Nucl. Mater.* **363–365** 12
[5] Vulliez K. *et al* 2003 *Fusion Eng. Des.* **66–68** 531
[6] Bosia G. *et al* 2003 *Fusion Sci. Technol.* **43** 153
[7] Vulliez K. *et al* 2008 *Nucl. Fusion* **48** 065007
[8] Gargiulo L. *et al* 2007 *Fusion Eng. Des.* **82** 1996
[9] Houry M. 2008 Development and operation of an ITER relevant inspection robot *22nd IAEA Fusion Energy Conf. (Geneva, Switzerland, 13–18 October 2008)* Paper FT/P2-18 http://www-naweb.iaea.org/napc/physics/FEC/FEC2008/html/index.htm
[10] Roth J. *et al* 2008 *Plasma Phys. Control. Fusion* **50** 103001
[11] Loarer T. *et al* 2007 *Nucl. Fusion* **47** 1112
[12] Pégourié B. *et al* 2009 Overview of the deuterium inventory campaign in Tore Supra: Operational conditions and particle balance *J. Nucl. Mater.* submitted
[13] Tsitrone E. *et al* 2009 *Nucl. Fusion* **49** 075011
[14] Ekedahl A. *et al* 2007 *Proc. 17th Topical Conf. on Radiofrequency Power in Plasmas (Clearwater, Florida, 2007) AIP Conf. Proc.* **933** 237 http://proceedings.aip.org/proceedings/confproceed/933.jsp
[15] Ekedahl A. *et al* 2009 *Nucl. Fusion* **49** 095010
[16] Lennholm M. *et al* 2009 *Phys. Rev. Lett.* **102** 115004
[17] Lennholm M. *et al* 2009 *Fusion Sci. Technol.* **55** 45
[18] Gribov Y. *et al* 2007 *Nucl. Fusion* **47** S385
[19] Bucalossi J. 2008 *Nucl. Fusion* **48** 054005
[20] Sabot R. *et al* 2006 *Plasma Phys. Control. Fusion* **48** B421
[21] Chatelier M. *et al* 2007 *Nucl. Fusion* **47** S579
[22] Urano H. *et al* 2006 *Nucl. Fusion* **46** 781
[23] Vermare L. *et al* 2007 *Nucl. Fusion* **47** 490
[24] McDonald D.C. *et al* 2008 *Plasma Phys. Control. Fusion* **50** 124013
[25] Gerbaud T. *et al* 2008 *Controlled Fusion and Plasma Physics* (Geneva: EPS) P1.044
[26] Perkins F.W. *et al* 1993 *Phys. Fluids* B **5** 477
[27] Petty C.C. and Luce T.C. 1999 *Phys. Plasmas* **6** 909
[28] Zou X.L. *et al* 2008 *Controlled Fusion and Plasma Physics* (Geneva: EPS) D4.004
[29] Parisot T. *et al* 2008 *Plasma Phys. Control. Fusion* **50** 055010
[30] Guirlet R. *et al* 2008 *Controlled Fusion and Plasma Physics* (Geneva: EPS) O4.050
[31] Bourdelle C. *et al* 2007 *Phys. Plasmas* **14** 112501
[32] Kočan M. *et al* 2009 Measurements of scrape-off-layer ion-to-electron temperature ratio in Tore Supra ohmic plasmas *J. Nucl. Mater.* submitted
[33] Gunn J.P. *et al* 2008 Suprathermal electron beams and large sheath potentials generated by RF-antennae in the scrape-off layer of Tore Supra *22nd IAEA Fusion Energy Conf. (Geneva, Switzerland, 13–18 October 2008)* (Vienna: IAEA) CD-ROM file EX/P6-32 and http://www-naweb.iaea.org/napc/physics/FEC/FEC2008/html/index.htm
[34] Jacquet P. *et al* 1999 *Phys. Plasmas* **6** 214
[35] Maget P. *et al* 2004 *Nucl. Fusion* **44** 443
[36] Lütjens H. and Luciani J.F. 2008 *J. Comput. Phys.* **227** 6944
[37] Maget P. *et al* 2007 *Phys. Plasmas* **14** 052509
[38] Maget P. *et al* 2007 *Nucl. Fusion* **47** 233
[39] Turco F. *et al* 2008 *Plasma Phys. Control. Fusion* **50** 035001
[40] Basiuk V. *et al* 2003 *Nucl. Fusion* **43** 822
[41] Sabot R. *et al* 2009 *Nucl. Fusion* **49** 085033
[42] Udintsev V.S. *et al* 2006 *Plasma Phys. Control. Fusion* **48** L33
[43] Goniche M. *et al* 2008 *Fusion Sci. Technol.* **53** 88
[44] Macor A. *et al* 2009 Redistribution of suprathermal electrons due to fishbone frequency jumps *Phys. Rev. Lett.* at press
[45] Zonca F. *et al* 2007 *Nucl. Fusion* **47** 1588
[46] Giruzzi G. *et al* 2003 *Phys. Rev. Lett.* **91** 135001
[47] Beaumont B. *et al* 2001 *Fusion Eng. Des.* **56–57** 667
[48] Hoang G.T. *et al* 1994 *Nucl. Fusion* **34** 75
[49] Garcia J. *et al* 2003 *Phys. Rev. Lett.* **100** 255004
[50] Artaud J.F. *et al* 2008 *Controlled Fusion and Plasma Physics* (Geneva: EPS) P5.068